NOAA Technical Report NESS 72

An Intercomparison of Radiosonde and Satellite-Derived Cross Sections During the AMTEX

W. C. SHEN, W. L. SMITH, AND H. M. WOOLF

WASHINGTON, D.C.
FEBRUARY 1975

noaa NATIONAL OCEANIC AND ATMOSPHERIC ADMINISTRATION / National Environmental Satellite Service

NOAA TECHNICAL REPORTS

National Environmental Satellite Service Series

The National Environmental Satellite Service (NESS) is responsible for the establishment and operation of the environmental satellite systems of NOAA.

Publication of a report in NOAA Technical Report NESS series will not preclude later publication in an expanded or modified form in scientific journals. NESS series of NOAA Technical Reports is a continuation of, and retains the consecutive numbering sequence of, the former series, ESSA Technical Report National Environmental Satellite Center (NESC), and of the earlier series, Weather Bureau Meteorological Satellite Laboratory (MSL) Report. Reports 1 through 39 are listed in publication NESC 56 of this series.

Reports 1 through 50 in the series are available from the National Technical Information Service (NTIS), U.S. Department of Commerce, Sills Bldg., 5285 Port Royal Road, Springfield, Va. 22151, in paper copy or microfiche form. Order by accession number, when given, in parentheses. Beginning with 51, printed copies of the reports are available through the Superintendent of Documents, U.S. Government Printing Office, Washington, D.C. 20402; microfiche available from NTIS (use accession number when available). Prices given on request from the Superintendent of Documents or NTIS.

ESSA Technical Reports

NESC 40 Cloud Measurements Using Aircraft Time-Lapse Photography. Linwood F. Whitney, Jr., and E. Paul McClain, April 1967, 24 pp. (PB-174-728)

NESC 41 The SINAP Problem: Present Status and Future Prospects; Proceedings of a Conference Held at the National Environmental Satellite Center, Suitland, Maryland, January 18-20, 1967. E. Paul McClain, October 1967, 26 pp. (PB-176-570)

NESC 42 Operational Processing of Low Resolution Infrared (LRIR) Data From ESSA Satellites. Louis Rubin, February 1968, 37 pp. (PB-178-123)

NESC 43 Atlas of World Maps of Long-Wave Radiation and Albedo--for Seasons and Months Based on Measurements From TIROS IV and TIROS VII. J. S. Winston and V. Ray Taylor, September 1967, 32 pp. (PB-176-569)

NESC 44 Processing and Display Experiments Using Digitized ATS-1 Spin Scan Camera Data. M. B. Whitney, R. C. Doolittle, and B. Goddard, April 1968, 60 pp. (PB-178-424)

NESC 45 The Nature of Intermediate-Scale Cloud Spirals. Linwood F. Whitney, Jr., and Leroy D. Herman, May 1968, 69 pp. plus appendixes A and B. (AD-673-681)

NESC 46 Monthly and Seasonal Mean Global Charts of Brightness From ESSA 3 and ESSA 5 Digitized Pictures, February 1967-February 1968. V. Ray Taylor and Jay S. Winston, November 1968, 9 pp. plus 17 charts. (PB-180-717)

NESC 47 A Polynomial Representation of Carbon Dioxide and Water Vapor Transmission. William L. Smith, February 1969 (reprinted April 1971), 20 pp. (PB-183-296)

NESC 48 Statistical Estimation of the Atmosphere's Geopotential Height Distribution From Satellite Radiation Measurements. William L. Smith, February 1969, 29 pp. (PB-183-297)

NESC 49 Synoptic/Dynamic Diagnosis of a Developing Low-Level Cyclone and Its Satellite-Viewed Cloud Patterns. Harold J. Brodrick and E. Paul McClain, May 1969, 26 pp. (PB-184-612)

NESC 50 Estimating Maximum Wind Speed of Tropical Storms From High Resolution Infrared Data. L. F. Hubert, A. Timchalk, and S. Fritz, May 1969, 33 pp. (PB-184-611)

NESC 51 Application of Meteorological Satellite Data in Analysis and Forecasting. Ralph K. Anderson, Jerome P. Ashman, Fred Bittner, Golden R. Farr, Edward W. Ferguson, Vincent J. Oliver, Arthur H. Smith, James F. W. Purdom, and Rance W. Skidmore, March 1974 (reprint and revision of NESC 51, September 1969, and inclusion of Supplement, November 1971, and Supplement 2, March 1973), pp. 1--6C-18 plus references.

NESC 52 Data Reduction Processes for Spinning Flat-Plate Satellite-Borne Radiometers. Torrence H. MacDonald, July 1970, 37 pp. (COM-71-00132)

(Continued on inside back cover)

NOAA Technical Report NESS 72

An Intercomparison of Radiosonde and Satellite-Derived Cross Sections During the AMTEX

W. C. SHEN, W. L. SMITH, AND H. M. WOOLF

WASHINGTON, D.C.
FEBRUARY 1975

UNITED STATES
DEPARTMENT OF COMMERCE
Frederick B. Dent, Secretary

NATIONAL OCEANIC AND
ATMOSPHERIC ADMINISTRATION
Robert M. White, Administrator

National Environmental
Satellite Service
David S. Johnson, Director

CONTENTS

Mention of a commercial company or product does not constitute an endorsement by the NOAA National Environmental Satellite Service. Use for publicity or advertising purposes of information from this publication concerning proprietary products or the tests of such products is not authorized.

For sale by the Superintendent of Documents, U.S. Government Printing Office, Washington, D.C., 20402. Price $0.65

AN INTERCOMPARISON OF RADIOSONDE AND SATELLITE-DERIVED CROSS SECTIONS DURING THE AMTEX

W.C. Shen, W.L. Smith, and H.M. Woolf
National Environmental Satellite Service, NOAA, Washington, D.C.

ABSTRACT. A comparison is made between zonal cross-sections of meteorological parameters obtained from Nimbus-5 radiance measurments and those observed by radiosondes during the Air Mass Transformation Experiment (AMTEX) during February 1974. The results of this limited case study (four orbits over the AMTEX area) show: (1) reasonable agreement between the total water vapor content derived from the Nimbus-5 Infrared Temperature Profile Radiometer (ITPR) and the Nimbus-E Microwave Spectrometer (NEMS) radiance data and that observed by radiosondes, (2) good agreement between the vertical cross-section of temperature derived from Nimbus-5 radiance data and vertical cross-sections obtained from radiosonde temperature observations, and (3) good agreement between the geostrophic wind distributions derived from the Nimbus-5 and radiosonde temperature data, both showing good correspondence to the actual wind observed by the radiosondes. The variation of outgoing longwave radiative flux and the cloud distribution derived from the ITPR data correspond well with the variation of cloudiness indicated on cloud photographs. These results indicate that the satellite observations should be useful during the AMTEX in February 1975.

I. INTRODUCTION

An Air Mass Transformation Experiment (AMTEX) was conducted over the East China Sea near Okinawa, Japan, from Feb. 14 to 28, 1974. The aim of this experiment (ICSU/WMO 1973) is to increase our understanding of the air-sea interaction that occurs during the modification of a cold polar continental air mass when it flows over the warm ocean.

During the AMTEX observational period, four orbits of the Nimbus-5 satellite were over the AMTEX area. Orbital number and the synoptic situation during the orbital traverses are in table 1.[1] Figure 1 shows the Nimbus-5 orbital tracks and the locations of nearby radiosonde stations. Note that the orbits of February 16, 18, and 23 were descending at night and the orbit of February 27 was ascending during the daytime over the AMTEX area.

[1]All tables and figures are grouped together at the back of the study.

The purpose of this study is to compare meteorological parameters derived from satellite radiance measurements with those derived from the conventional radiosondes to assess the usefulness of satellite observations for diagnosing the intense weather situation under study during AMTEX.

II. DATA

The various types of data used for this study are listed in table 2.

Further, one should indicate the inherent difference between a satellite sounding system and a conventional radiosonde. The satellite measurement is closely related to the mean temperature and total integrated water vapor of a volume of atmosphere with dimensions of several kilometers both horizontally and vertically. The radiosonde measures the temperature and water vapor state of small parcels of atmosphere. Although the radiosonde is capable of observing with much higher vertical resolution than is the remote satellite sounder (meters compared to kilometers), the satellite sounding system usually can achieve much higher spatial resolution and more meaningful horizontal gradients than those possible with a practical radiosonde network. The fact that the same instrument observes at all geographical locations contributes greatly to the relative accuracy of the satellite sounding system. During AMTEX, a special network of ship radiosonde stations made good horizontal coverage possible with a conventional radiosonde system. As a result, radiosonde as well as satellite soundings were obtained with a spacing generally less than 300 km.

III. RESULTS

Figures 2 through 5 show the distribution of atmospheric water vapor content, radiative flux of outgoing longwave radiation, and cloud cover as derived from the Nimbus-5 radiance measurements. Also shown is a pictorial image of the cloud distribution obtained from the 4-mi (6.4 km) resolution-scanning Temperature Humidity Infrared Radiometer (THIR) aboard Nimbus 5. The water vapor, cloud, and longwave flux quantities were derived from the Nimbus-5 sounding radiance data, using the procedures developed by Smith et al. (1974).

The retrieval of atmospheric water vapor content from the infrared radiances observed by the Infrared Temperature Profile Radiometer (ITPR) is performed in two steps. First, an initial estimate of the mixing ratio is obtained by application of regression equations relating water vapor mixing ratio to the radiances observed (a) in the 11-μm window, (b) in three semitransparent spectral regions of the 15-μm CO_2 band, and (c) in the rotational water vapor band at 20 μm. The regression relations are based on a climatological sample of radiosonde data and theoretical calculations of radiance. Second, the mixing ratio profile then is adjusted through an iterative solution until the difference between observed and calculated 20-μm radiances is reduced to the nominal instrumental noise level.

The total atmospheric water vapor content also is derived from the microwave radiance data from the Nimbus-E Microwave Spectrometer (NEMS). The brightness temperatures observed at 22.2 and 31.4 GHz together with the ITPR-derived surface temperature are used to estimate the total atmospheric absorption by liquid water and water vapor in those channels. The total water vapor and liquid water contents are computed from a pair of linear simultaneous equations involving the water vapor and liquid water absorptions at 22.2 and 31.4 GHz.

The total water vapor contents derived over the Kuroshio area are given in table 3. The total water vapor contents derived from the microwave sounder and from the ITPR are in good agreement with those obtained from the radiosondes. The NEMS total water vapor contents are generally larger then those of the ITPR because the microwave energy penetrates clouds and the water vapor content of clouds is usually larger than that of the surrounding clear air sampled by the infrared observations. Note that the total water vapor contents in the first 3 days (Feb. 16, 18, and 23) are 1 to 2 times higher then the day after the cold polar air outbreak (Feb. 27).

As shown in figures 2 through 5, the flux of outgoing longwave radiation derived from the ITPR radiance data has a large variation because of nonuniform temperature of the underlying surface and the varying heights and amounts of cloud. The low radiation fluxes are associated with high dense clouds or low surface temperatures in the north. On Feb. 16, 1974, there were three areas of low outgoing radiation flux located near 25°N, 35°N, and 50°N. The positions of these radiation minimums agree with the frontal cloud systems indicated on the National Meteorological Center (NMC), Suitland, Md., operational surface synoptic map (not shown) and also on the THIR cloud image.

The lowest flux--360 ly/day--was observed in the AMTEX area on February 23 just before the outbreak of the cold polar air mass. This low flux was due to the cloudiness associated with the intense cold front extending from an active cyclone located to the southeast of Japan. The maximum outgoing radiation flux of 600 ly/day observed in the AMTEX area occurred under clear-sky conditions on February 16 and 18.

The algorithm used in the inversion of the radiative transfer equation to obtain atmospheric temperatures from the Nimbus-5 radiance measurements is the multiple-channel approach of Smith et al. (1974). Infrared radiances from six channels in the ITPR and two channels of the SCR (Selective Chopper Radiometer) were combined with microwave brightness temperatures observed in three oxygen-absorption channels by the NEMS. From this set of measurements covering different spectral regions, the temperature is specified for 25 levels from Earth's surface to the upper stratosphere (0.1 mb). The temperature retrieval method employs the "minimum information solution" that minimizes the perturbation of an initial profile required to satisfy the complete set of outgoing radiance measurements to within their instrumental noise levels. The initial temperature profile is generated by regression equations derived from a climatological sample of radiosonde data. Consequently, the Nimbus retriev-

als are independent of either contemporary radiosonde or numerical model (forecast) information.

Figures 6 through 9 show the meridional temperature cross sections, plotted from 20°N to 50°N and from 1000 mb to 10 mb. There are three parts in each figure. Part (A) shows the radiosonde temperature observations; part (B), the original temperatures derived from Nimbus 5 (ITPR+NEMS+SCR) radiation measurements; and part (C), the Nimbus-5 temperatures after correcting for systematic differences between the Nimbus and radiosonde level temperatures (i.e., the removal of the level mean error).

The pattern of the Nimbus-5 temperatures follows closely those of the radiosondes. There is generally better correspondence between the two fields of temperature gradients than between their absolute values. In fact, by removing the level mean difference between the satellite and radiosonde temperatures, good agreement is obtained between the satellite and the radiosonde cross-sections.

Perhaps the best way to determine how well the thermal field derived from the Nimbus data describes the state of the atmosphere is to compare the geostrophic wind distribution obtained from it with the geostrophic wind obtained from the radiosonde temperature profiles and with the true wind distribution also observed by the rawinsonde. (The geostrophic winds were computed assuming zero wind velocity at the 1000-mb level.)

Figures 10 through 13 show a comparison of geostrophic winds derived from the Nimbus-5 temperatures, the radiosonde temperatures, and the radiosonde winds. (For locations of Nimbus-5 and radiosonde temperatures, see figs. 6 through 9.) The relatively good depiction of the wind field associated with the jet stream from the satellite data confirms the study based on theoretical computations presented by Togstad and Horn (1974). The latitude and altitude locations of the jet core (wind maximum) from the satellite-derived temperature profiles appear to be more accurate than the locations indicated by the radiosonde temperature profiles on 3 of the 4 days studied, despite a 3-hr time difference between the satellite and radiosonde observations. Table 4 summarizes the major jet stream features shown in figures 10 through 13.

The reason for the higher accuracy of the satellite data for locating the jet core geographically is probably a result of the relatively high density of Nimbus-5 soundings as compared to coarsely spaced radiosondes along the suborbital track. The reason for somewhat better altitude positioning of the jet core is not entirely clear. The satellite-derived vertical profiles generally smooth the sharp discontinuities of atmospheric temperature observed by the radiosonde near the tropopause where the jet core is found. Possibly, the smoothing helps alleviate error amplification caused by the finite difference approximation used in the numerical computation of the geostrophic wind. In any case, the results shown in figures 10 through 13 certainly indicate that the tropopause smoothing inherent in

computing the satellite profiles has no adverse effect on defining the location of the jet core.

Note that, on February 16 and 23 (figs. 10 and 12), both the satellite- and radiosonde-derived geostrophic winds show a double maximum indicating the existence of two jet cores. This is not verified by the actual zonal wind distribution; however, two cirrus cloud streaks on February 23 are evident in the THIR photograph and in the ITPR-deduced cloudiness (fig. 4) at the locations shown in figure 12(B). The cores of maximum wind are to the north of the extensive cirrus bands near 30°N and 35°N along the satellite track. Thus the cirrus cloud streaks and the thermal winds indicate two cores of maximum wind instead of a single one as deduced from the rawinsonde data. The inability to diagnose the two jet cores from the rawinsonde data may be due to the horizontal spacing of the observations [see figs. 1 and 8(A)].

IV. CONCLUSIONS

A comparison of meteorological parameters derived from the Nimbus-5 radiance measurements with those of the radiosondes for 4 days during AMTEX has been made. This fairly limited analysis indicates:

1. The total water vapor contents derived from the Nimbus-5 ITPR and the NEMS are in fair agreement with each other and with measurements by radiosondes. All observations show that, during the cold polar air outbreak, the total water vapor content over the Kuroshio region was close to 1 g/cm^2. Prior to the cold air outbreak, the total water vapor content was about 3 g/cm^2 in the same region.

2. The regions of low outgoing longwave radiative flux correspond well with the areas of deepest convection indicated on cloud photographs.

3. A good agreement exists between the vertical cross-sections of temperatures derived from the satellite and from the radiosonde observations.

4. The geostrophic zonal wind distribution associated with the jet stream can be diagnosed accurately from the satellite temperature retrieval data. (The Nimbus-5 geostrophic zonal wind appears to have somewhat better correspondence with the actual zonal wind distribution than that derived from radiosonde temperature data, possibly because of the differences in observation density.) The inherent smoothing of the vertical temperature curve that occurs in the tropopause region does not seem to degrade the satellite-inferred geostrophic winds near the jet core.

ACKNOWLEDGMENTS

The authors wish to extend thanks to Y. Mitsuta of Kyoto University, Japan, for supplying 10-day mean sea surface temperatures and emagrams. We also appreciate the contribution of

L. Mannello who plotted and analyzed the thermal cross-sections and W. O'Tormey who prepared the data for computer processing. Our thanks also go to R. Ryan and L. Hatton for drafting the figures and to M. Schwier for typing the manuscript.

REFERENCES

ICSU/WMO (International Council of Scientific Unions/World Meteorological Organization), "The Air-Mass Transformation Experiment," GARP Publication Series No. 13, the Global Atmospheric Research Program, World Meteorological Organization, Geneva, Switzerland, 1973, 54 pp.

Smith, W.L., Woolf, H.M., Abel, P.G., Hayden, C.M., Chalfant, M., and Grody, N., "Nimbus-5 Sounder Data Processing System, Part I: Measurement Characteristics and Data Reduction Procedures," NOAA Technical Memorandum NESS 57, National Environmental Satellite Service, National Oceanic and Atmospheric Administration, U.S. Department of Commerce, Washington, D.C., June 1974, 99 pp.

Togstad, William E., and Horn, Lyle H., "An Application of the Satellite Indirect Sounding Technique in Describing the Hyperbaroclinic Zone of a Jet Streak," Journal of Applied Meteorology, Vol. 13, No. 2, Mar. 1974, pp. 264-276.

Table 1.--Orbital number and the synoptic situation

Feb. 1974	Orbit	Time (UT)*	Synoptic situation
16	5804	1509-1517	Weak monsoon and warm weather. A cold front passed through the AMTEX area at 1200 Z.
18	5830	1525-1534	Weak monsoon. A migratory anticyclone centered over the Sea of Japan.
23	5897	1512-1521	Weak monsoon. An intense cold front passed through the AMTEX area between 0600 Z and 1200 Z. A strong anticyclone, however, built up over Siberia; the anticyclone was ready to sweep over China.
27	5944	0242-0251	An open and closed cell cumulus convection was observed in the AMTEX area after a polar air outbreak.

*Universal Time (UT) is equivalent to Z or Greenwich Meridian Time (GMT).

Table 2.--Data sources

Nimbus-5 satellite radiances
ITPR (Infrared Temperature Profile Radiometer)
NEMS (Nimbus-E Microwave Spectrometer)
SCR (Selective Chopper Radiometer)
THIR (Temperature Humidity Infrared Radiometer)
Conventional
Ten-day mean sea surface temperatures
Surface observations (pressure, temperature, humidity, clouds)
Radiosonde (pressure, temperature, dew-point depression, wind)
National Meteorological Center (NMC) objective analyses

Table 3.--Total water vapor content (g/cm^2) over the Kuroshio region

Feb. 1974	Synoptic condition	NEMS	ITPR	RAOB*
16	Quiet period	2.9	2.6	2.8
18	Quiet period	2.6	1.9	2.3
23	Prior to polar air outbreak	3.5	2.2	2.9
27	After polar air outbreak	1.3	1.4	1.0

*Radiosonde Observation

Table 4.--Major features of the observed (true), radiosonde derived (geostrophic), and satellite derived (geostrophic) zonal wind distributions*

	Altitude of max wind (mb)			Latitude of max wind (°)			Intensity (m/s)		
Feb. 1974	Obs	Sat	RAOB	Obs	Sat	RAOB	Obs	Sat	RAOB
16	275	250	175	33	34	31	70	90	90
18	225	225	175	30	32	35	70	80	70
23	250	250	250	38	34	41	60	80	80
27	250	250	250	31	31	33	80	90	80

*Obs is observed; Sat, satellite; and max, maximum.

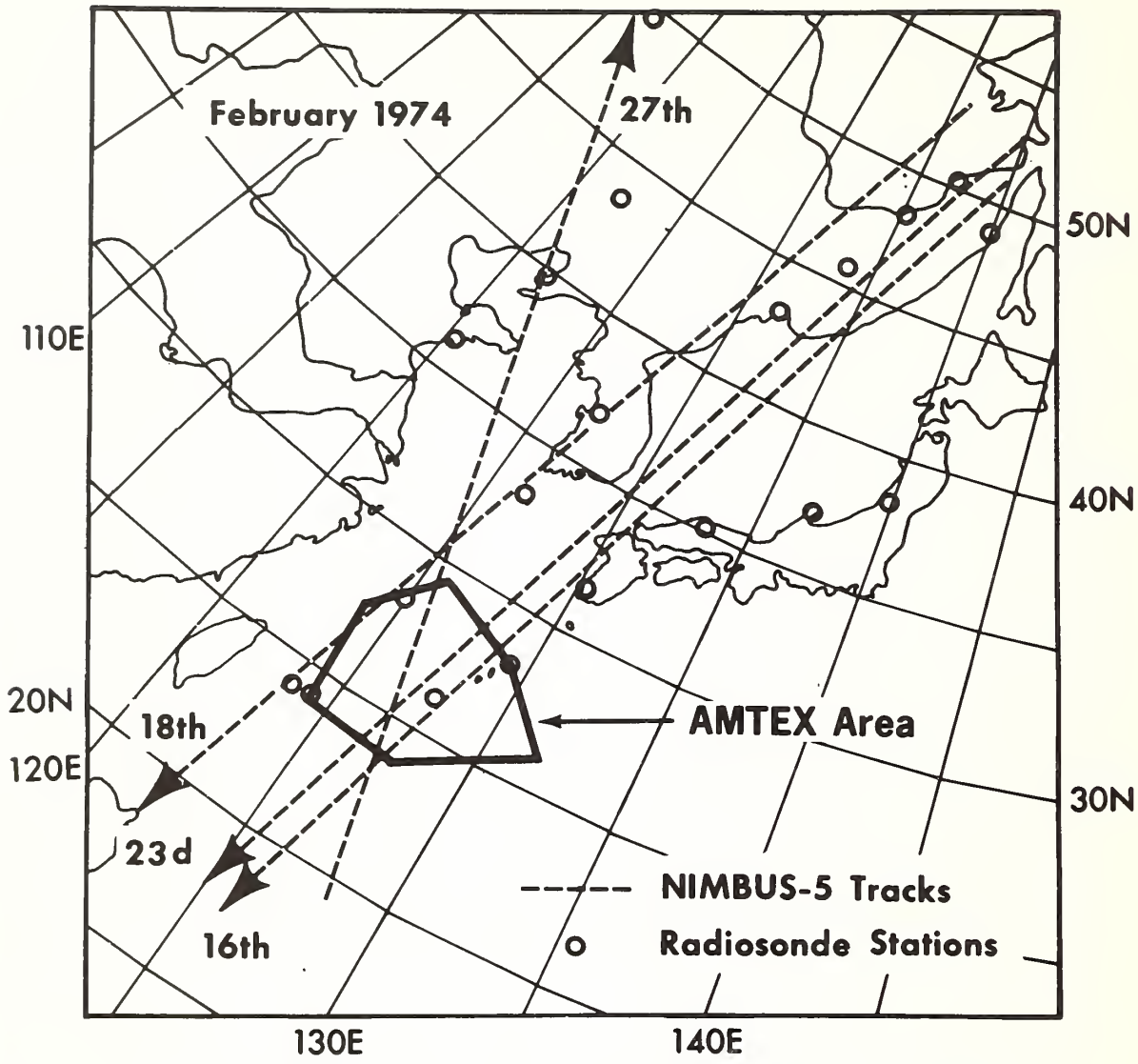

Figure 1.--Geographical locations of radiosonde and Nimbus-5 soundings

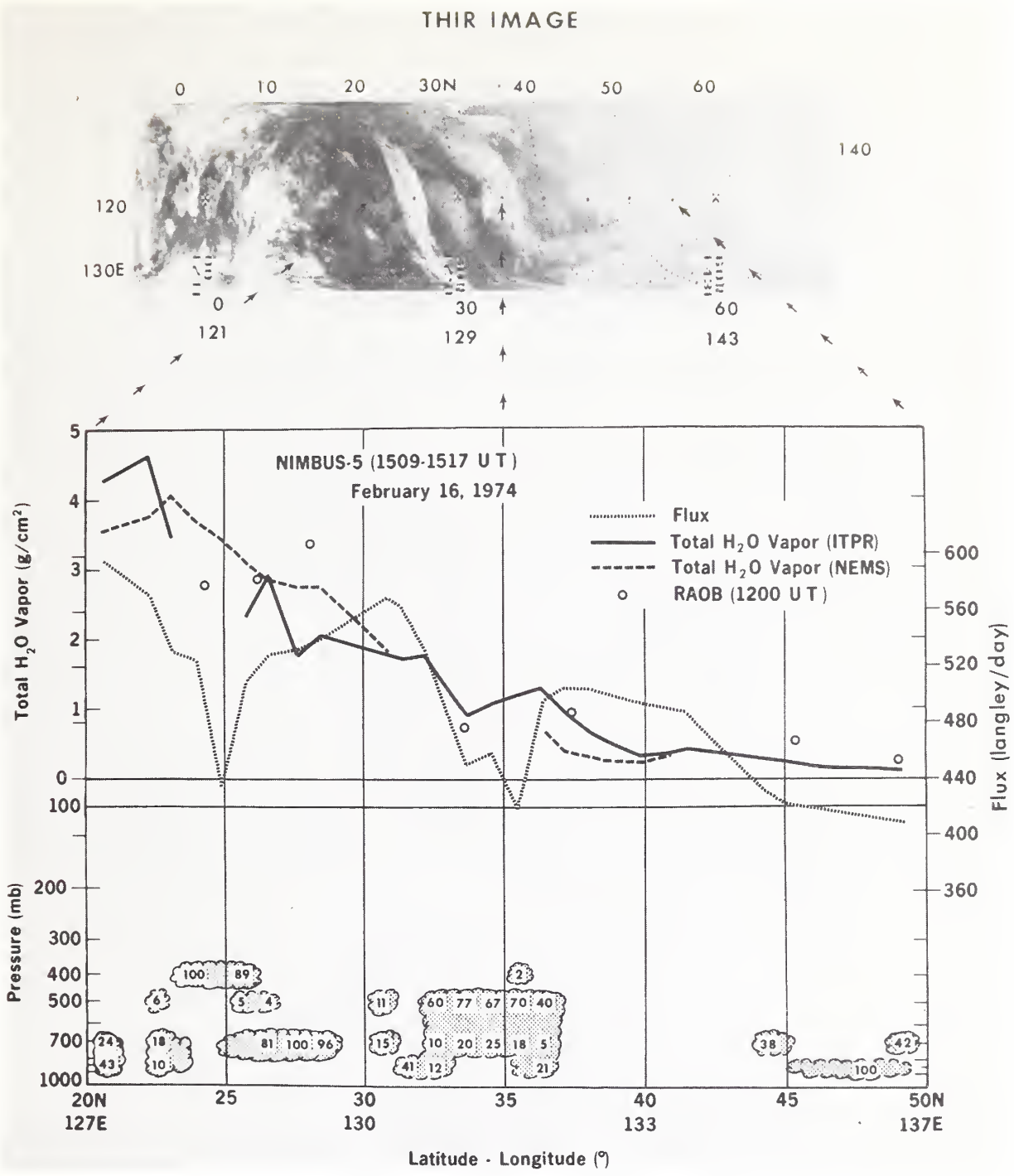

Figure 2.--Distribution of cloud amount, cloud height, water vapor content (g/cm^2), and outgoing longwave flux (ly/day) derived from the Nimbus-5 radiance measurements along the orbital track for Feb. 16, 1974

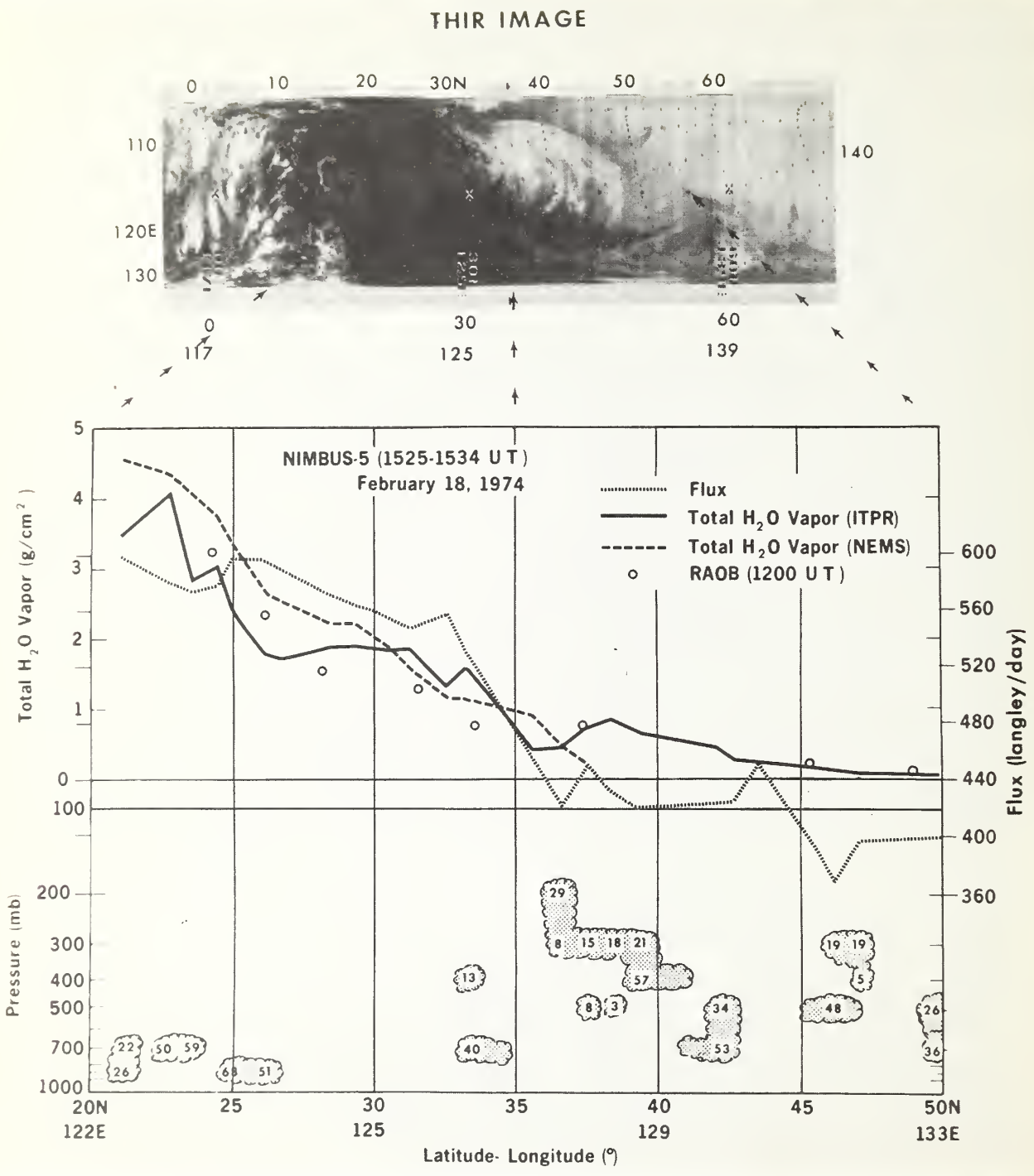

Figure 3.--Same as figure 2 except this is for Feb. 18, 1974

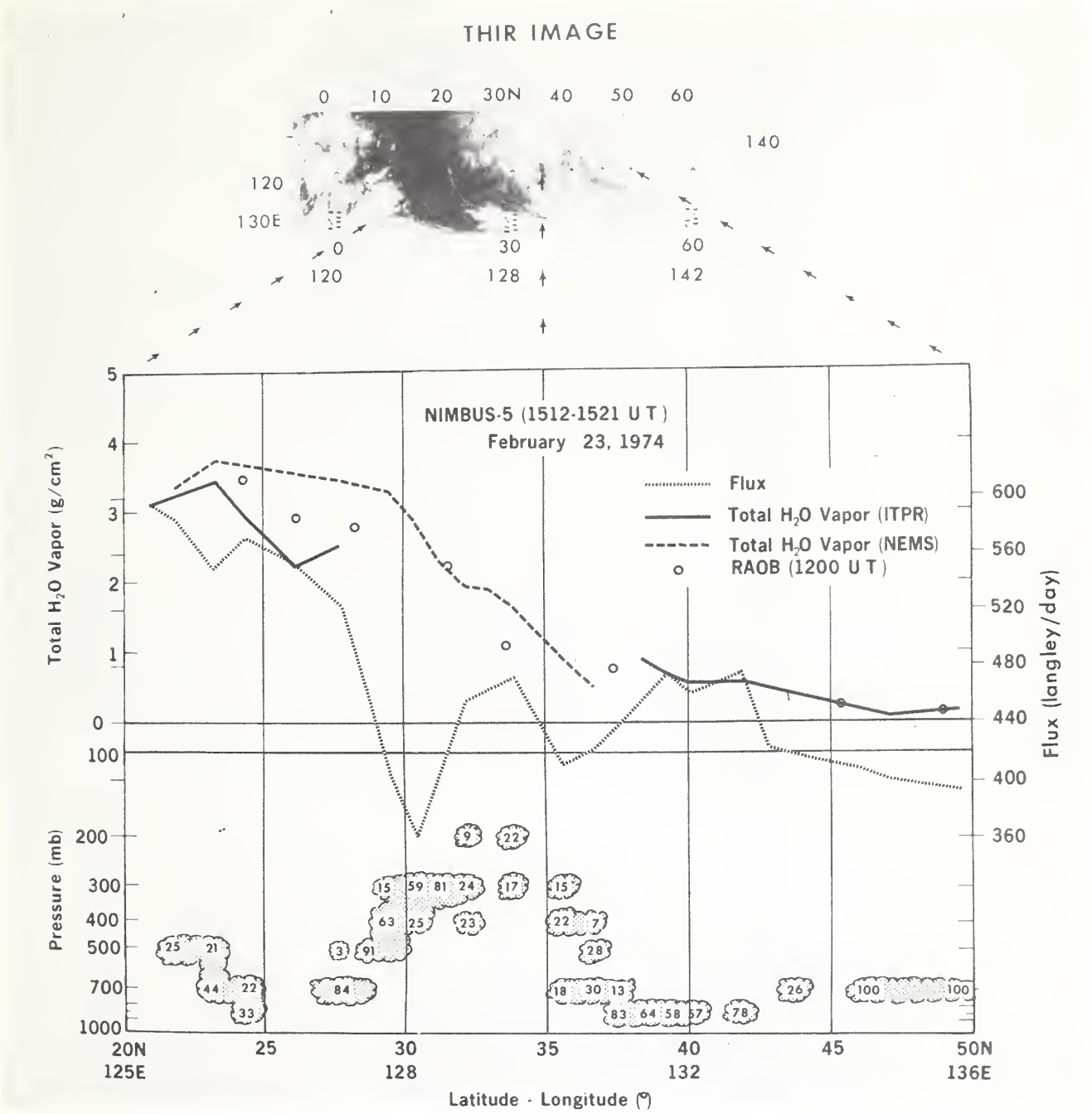

Figure 4.--Same as figure 2 except this is for Feb. 23, 1974

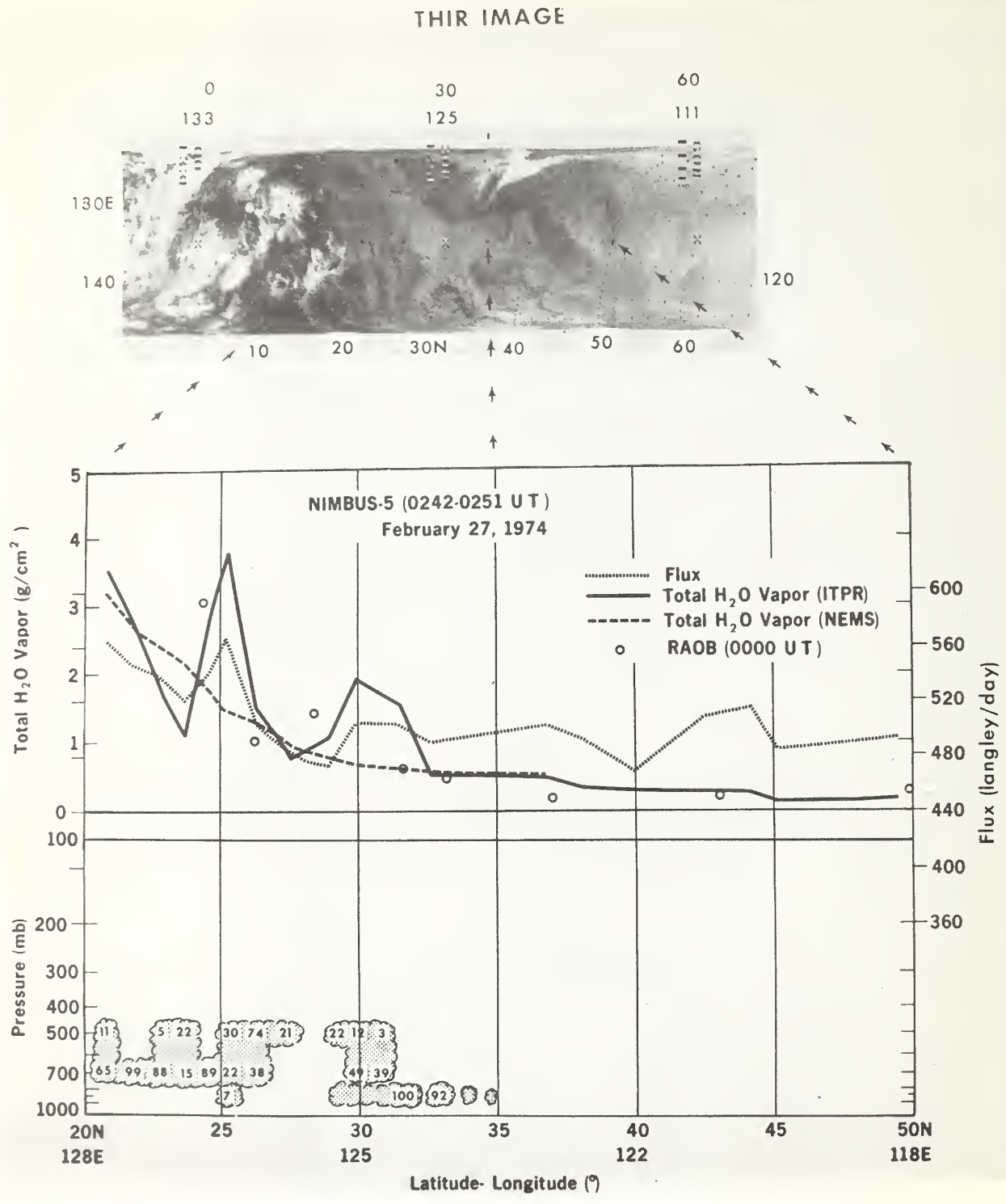

Figure 5.--Same as figure 2 except this is for Feb. 27, 1974

Temperature Cross Sections, °C

February 16, 1974

Ⓐ RAOB, 1200 U T

Ⓑ NIMBUS-5 , 1509-1517 U T

Ⓒ NIMBUS-5, with Mean Error Removed

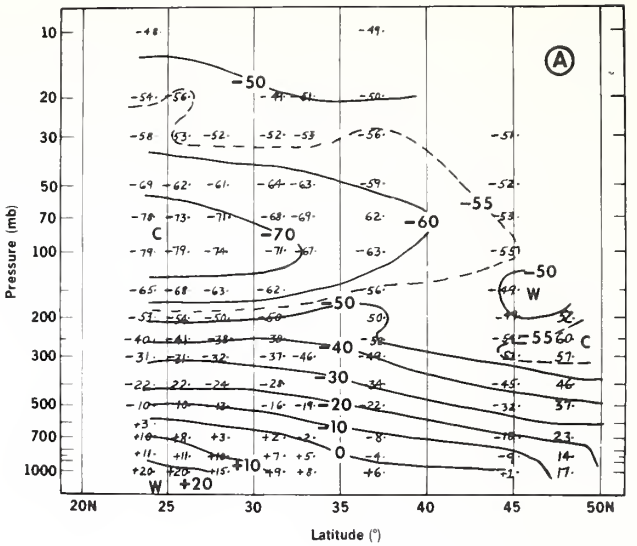

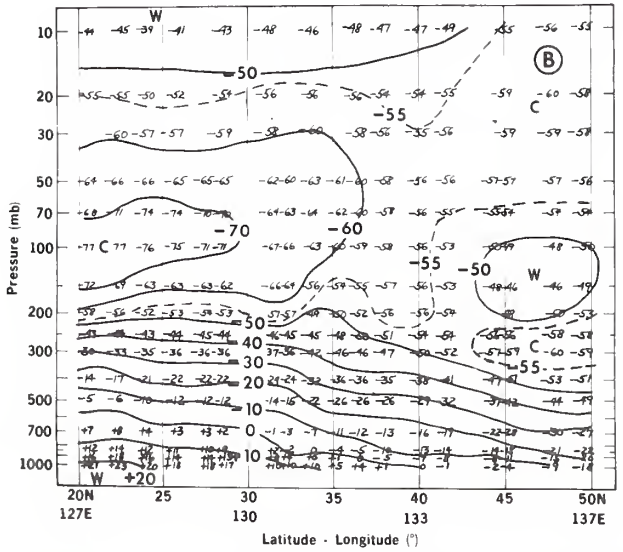

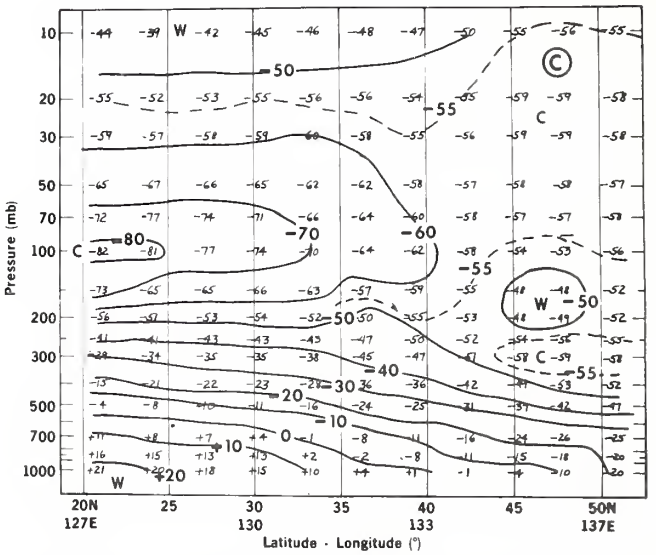

Figure 6.--Cross sections of temperatures for Feb. 16, 1974: (A) radiosonde temperatures; (B) Nimbus-5 temperatures, and (C) mean error removed temperatures

Temperature Cross Sections, °C

February 18, 1974

Ⓐ RAOB, 1200 U T

Ⓑ NIMBUS-5, 1525-1534 U T

Ⓒ NIMBUS-5, with Mean Error Removed

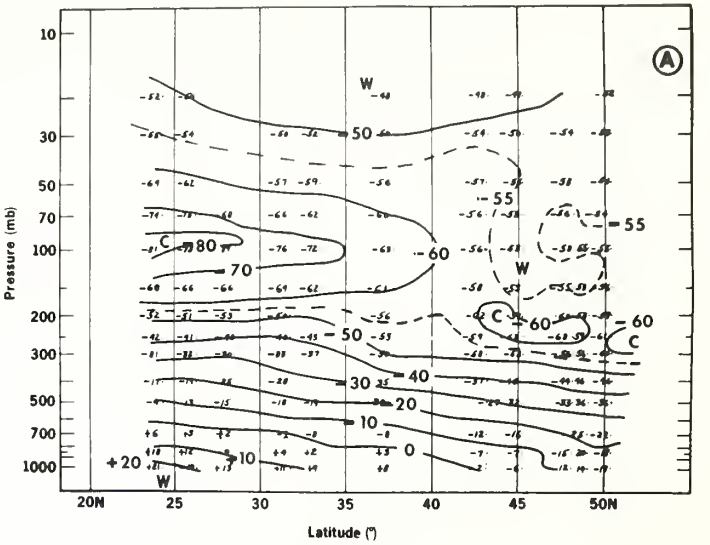

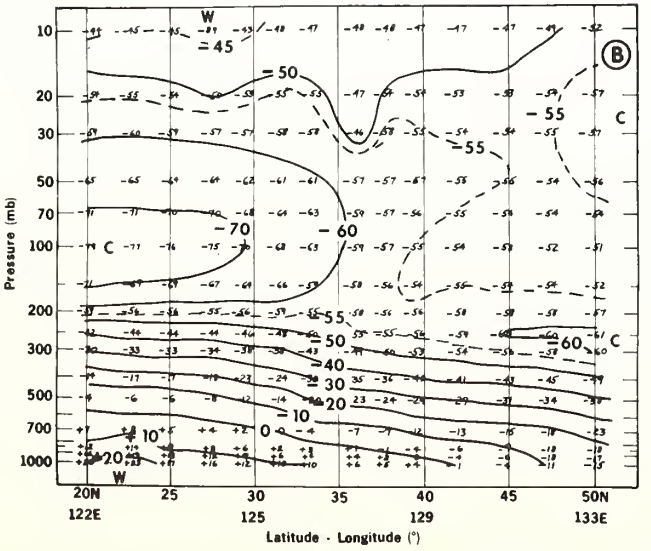

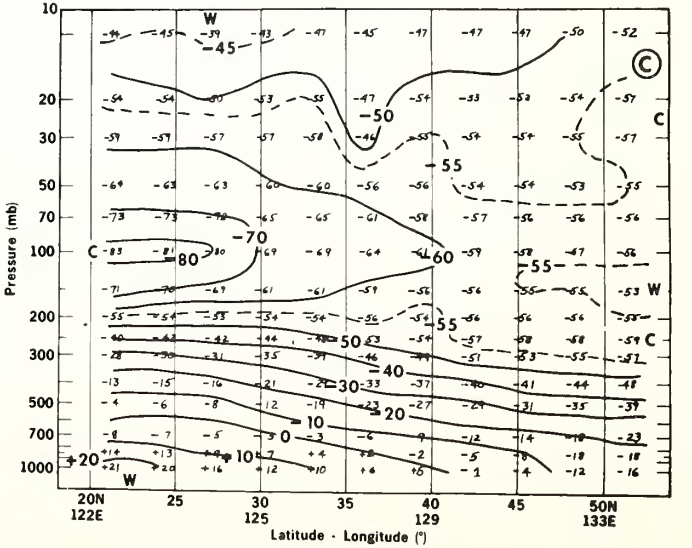

Figure 7.--Same as figure 6 except this is for Feb. 18, 1974

Temperature Cross Sections, °C

February 23, 1974

Ⓐ RAOB, 1200 U T

Ⓑ NIMBUS-5, 1512-1521 U T

Ⓒ NIMBUS-5, with Mean Error Removed

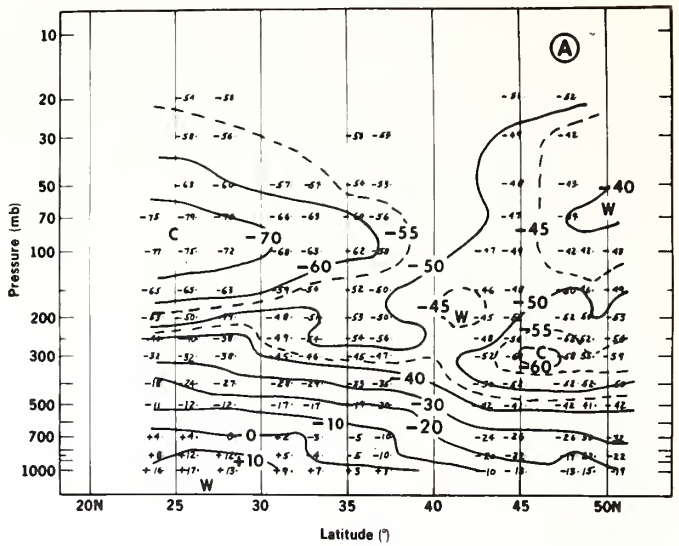

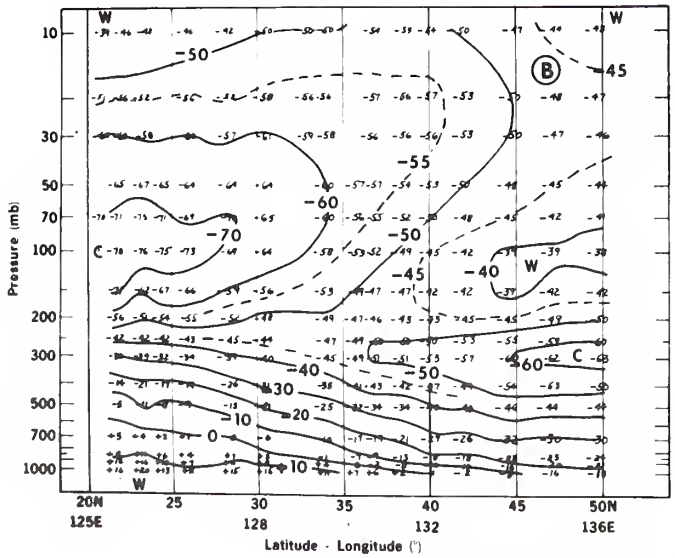

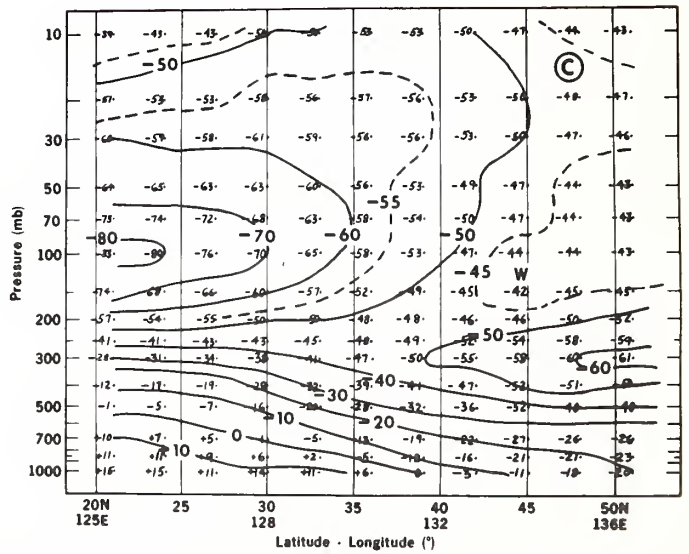

Figure 8.--Same as figure 6 except this is for Feb. 23, 1974

Temperature Cross Sections, °C

February 27, 1974

Ⓐ RAOB, 0000 UT

Ⓑ NIMBUS-5, 0242-0251 UT

Ⓒ NIMBUS-5, with Mean Error Removed

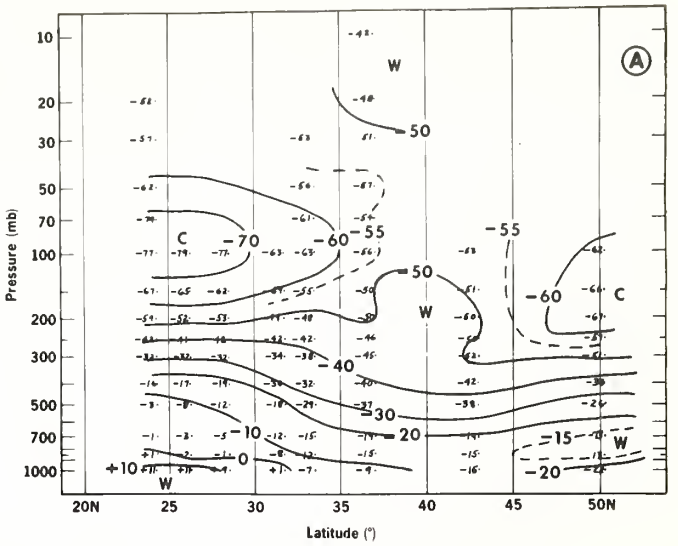

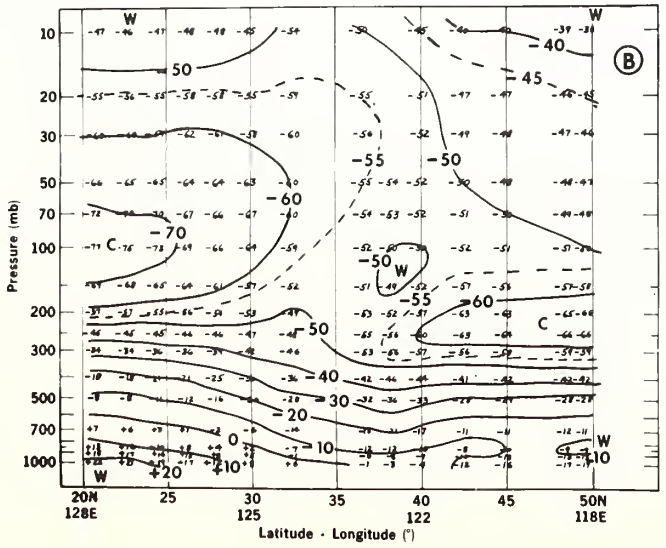

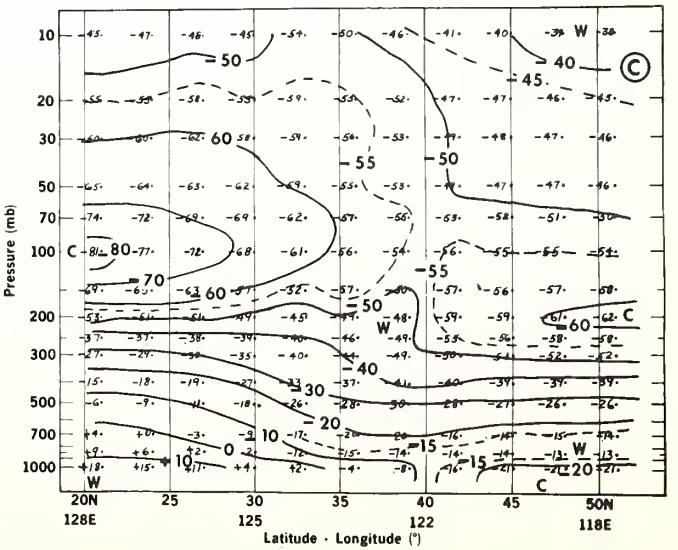

Figure 9.--Same as figure 6 except this is for Feb. 27, 1974

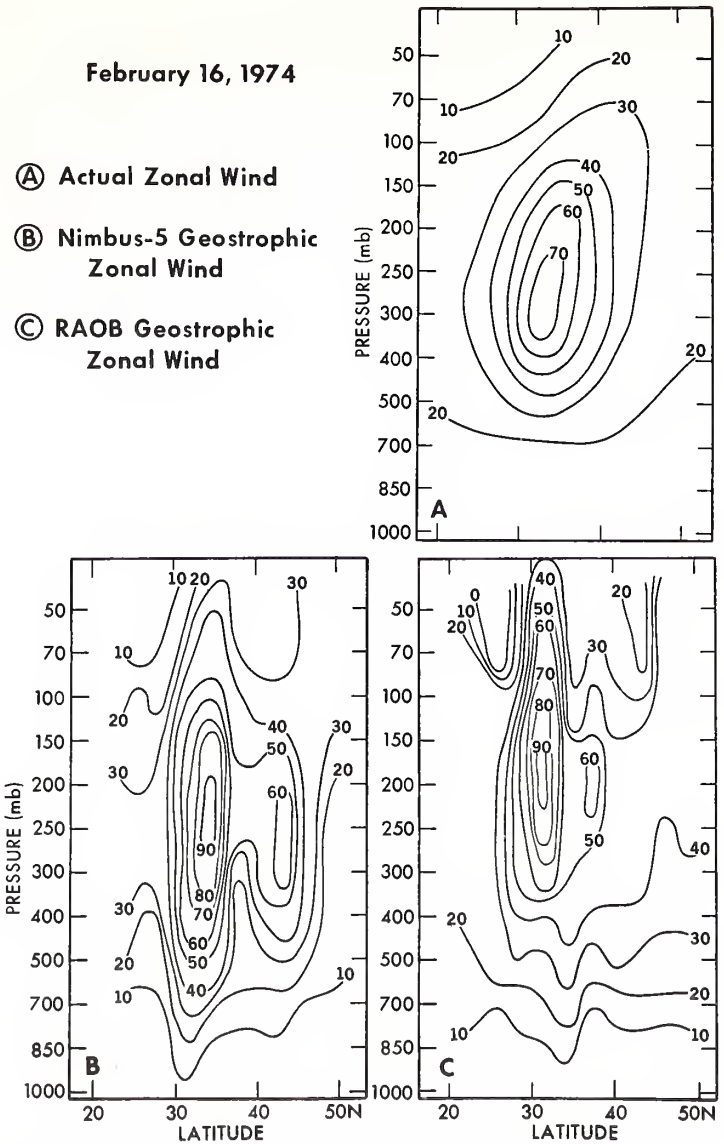

Figure 10.--Geostrophic zonal winds calculated from the radiosonde and Nimbus-5 temperatures and the zonal component of the true wind for Feb. 16, 1974

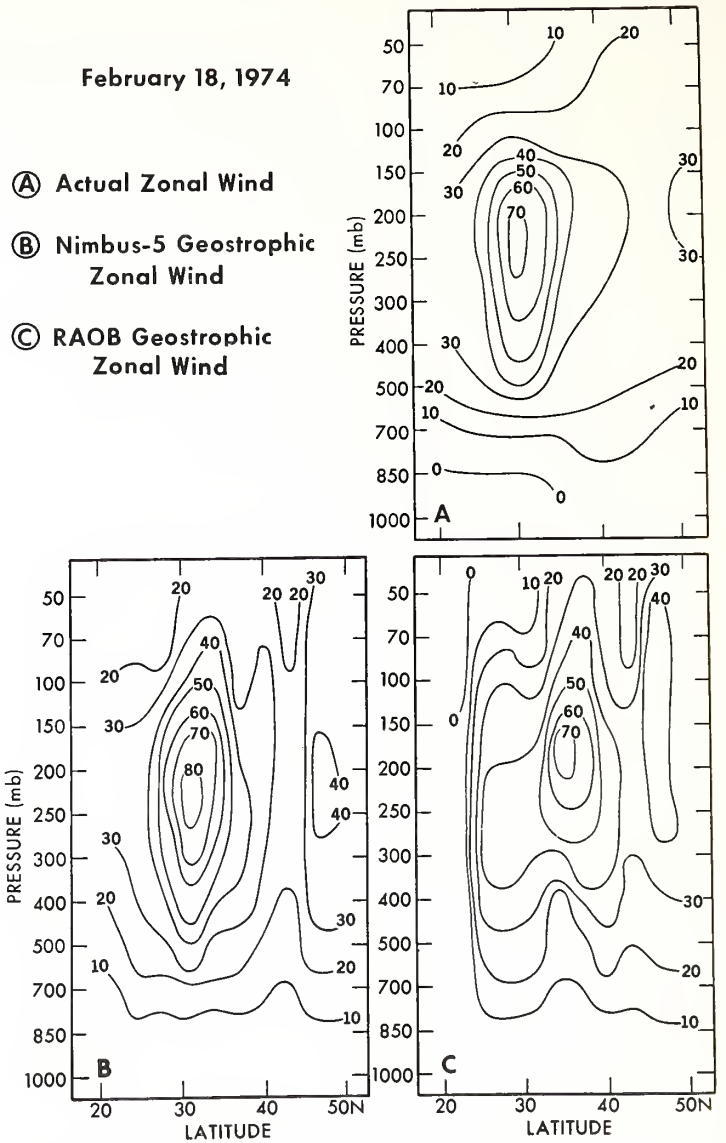

Figure 11.--Same as figure 10 except this is for Feb. 18, 1974

February 23, 1974

Ⓐ Actual Zonal Wind

Ⓑ Nimbus-5 Geostrophic Zonal Wind

Ⓒ RAOB Geostrophic Zonal Wind

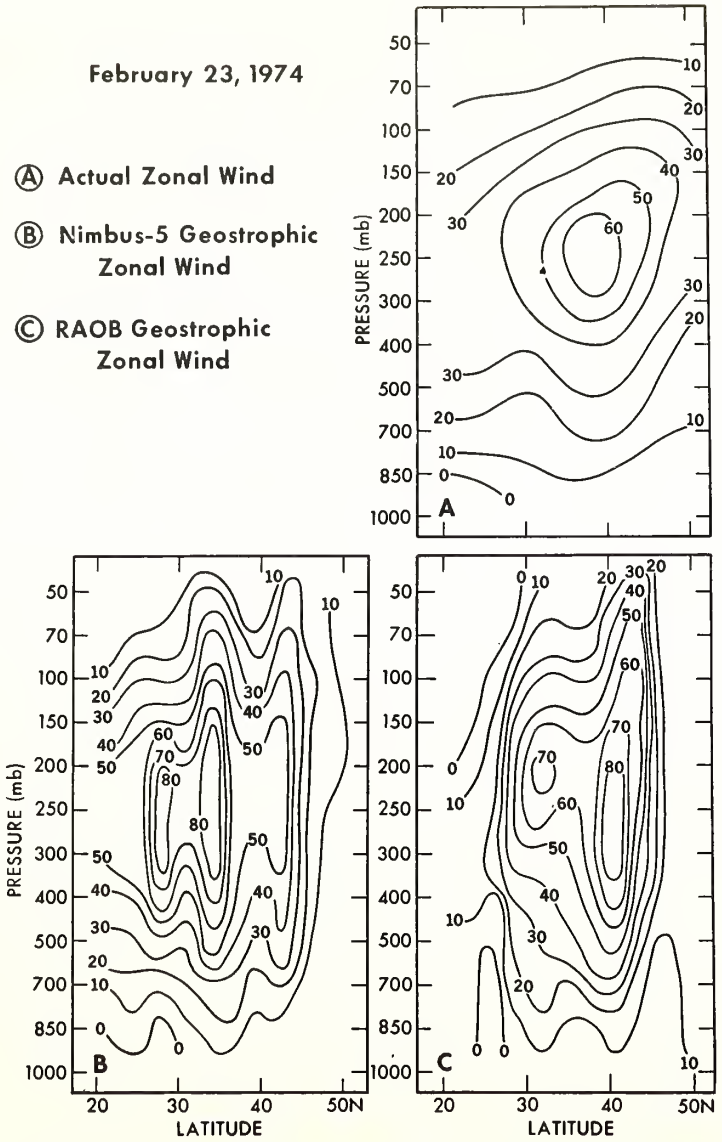

Figure 12.--Same as figure 10 except this is for Feb. 23, 1974

February 27, 1974

Ⓐ Actual Zonal Wind

Ⓑ Nimbus-5 Geostrophic Zonal Wind

Ⓒ RAOB Geostrophic Zonal Wind

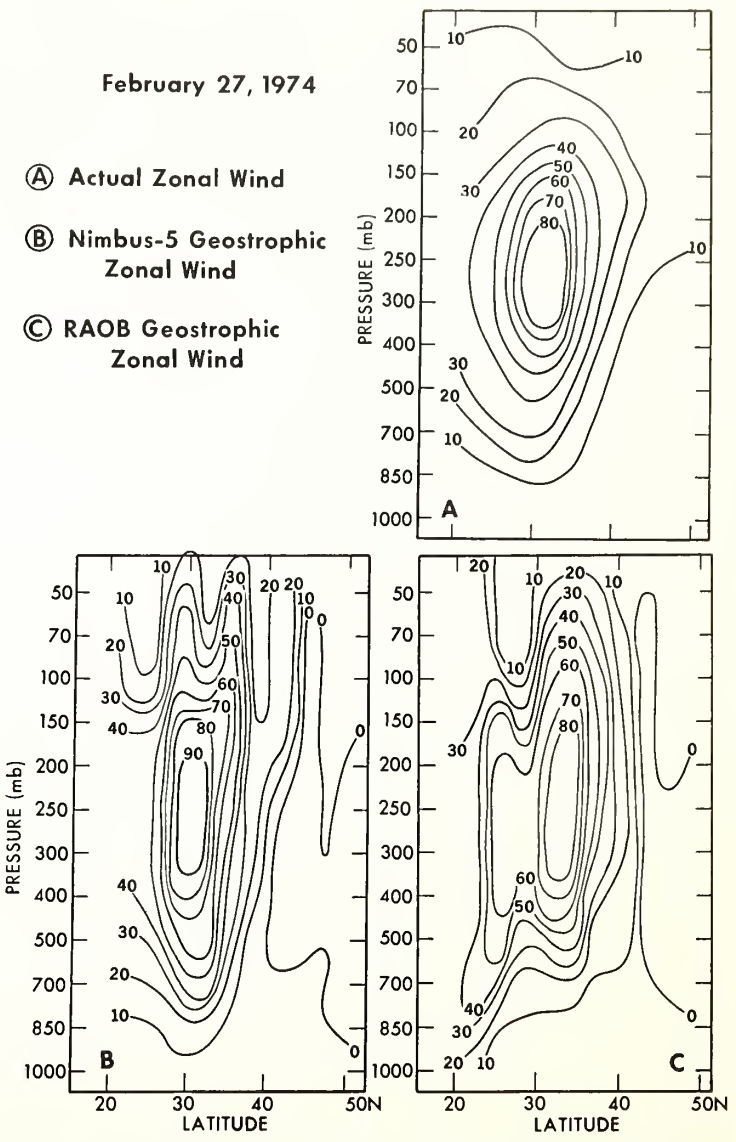

Figure 13.--Same as figure 10 except this is for Feb. 27, 1974

(Continued from inside front cover)

NESC 53 Archiving and Climatological Applications of Meteorological Satellite Data. John A. Leese, Arthur L. Booth, and Frederick A. Godshall, July 1970, pp. 1-1--5-8 plus references and appendixes A through D. (COM-71-00076)

NESC 54 Estimating Cloud Amount and Height From Satellite Infrared Radiation Data. P. Krishna Rao, July 1970, 11 pp. (PB-194-685)

NESC 56 Time-Longitude Sections of Tropical Cloudiness (December 1966-November 1967). J. M. Wallace, July 1970, 37 pp. (COM-71-00131)

NOAA Technical Reports

NESS 55 The Use of Satellite-Observed Cloud Patterns in Northern Hemisphere 500-mb Numerical Analysis. Roland E. Nagle and Christopher M. Hayden, April 1971, 25 pp. plus appendixes A, B, and C. (COM-73-50262)

NESS 57 Table of Scattering Function of Infrared Radiation for Water Clouds. Giichi Yamamoto, Masayuki Tanaka, and Shoji Asano, April 1971, 8 pp. plus tables. (COM-71-50312)

NESS 58 The Airborne ITPR Brassboard Experiment. W. L. Smith, D. T. Hilleary, E. C. Baldwin, W. Jacob, H. Jacobowitz, G. Nelson, S. Soules, and D. Q. Wark, March 1972, 74 pp. (COM-72-10557)

NESS 59 Temperature Sounding From Satellites. S. Fritz, D. Q. Wark, H. E. Fleming, W. L. Smith, H. Jacobowitz, D. T. Hilleary, and J. C. Alishouse, July 1972, 49 pp. (COM-72-50963)

NESS 60 Satellite Measurements of Aerosol Backscattered Radiation From the Nimbus F Earth Radiation Budget Experiment. H. Jacobowitz, W. L. Smith, and A. J. Drummond, August 1972, 9 pp. (COM-72-51031)

NESS 61 The Measurement of Atmospheric Transmittance From Sun and Sky With an Infrared Vertical Sounder. W. L. Smith and H. B. Howell, September 1972, 16 pp. (COM-73-50020)

NESS 62 Proposed Calibration Target for the Visible Channel of a Satellite Radiometer. K. L. Coulson and H. Jacobowitz, October 1972, 27 pp. (COM-73-10143)

NESS 63 Verification of Operational SIRS B Temperature Retrievals. Harold J. Brodrick and Christopher M. Hayden, December 1972, 26 pp. (COM-73-50279)

NESS 64 Radiometric Techniques for Observing the Atmosphere From Aircraft. William L. Smith and Warren J. Jacob, January 1973, 12 pp. (COM-73-50376)

NESS 65 Satellite Infrared Soundings From NOAA Spacecraft. L. M. McMillin, D. Q. Wark, J.M. Siomkajlo, P. G. Abel, A. Werbowetzki, L. A. Lauritson, J. A. Pritchard, D. S. Crosby, H. M. Woolf, R. C. Luebbe, M. P. Weinreb, H. E. Fleming, F. E. Bittner, and C. M. Hayden, September 1973, 112 pp. (COM-73-50936/6AS)

NESS 66 Effects of Aerosols on the Determination of the Temperature of the Earth's Surface From Radiance Measurements at 11.2 μm. H. Jacobowitz and K. L. Coulson, September 1973, 18 pp. (COM-74-50013)

NESS 67 Vertical Resolution of Temperature Profiles for High Resolution Infrared Radiation Sounder (HIRS). Y. M. Chen, H. M. Woolf, and W. L. Smith, January 1974, 14 pp. (COM-74-50230)

NESS 68 Dependence of Antenna Temperature on the Polarization of Emitted Radiation for a Scanning Microwave Radiometer. Norman C. Grody, January 1974, 11 pp. (COM-74-50431/AS)

NESS 69 An Evaluation of May 1971 Satellite-Derived Sea Surface Temperatures for the Southern Hemisphere. P. Krishna Rao, April 1974, 13 pp. (COM-74-50643/AS)

NESS 70 Compatibility of Low-Cloud Vectors and Rawins for Synoptic Scale Analysis. L. F. Hubert and L. F. Whitney, Jr., October 1974, 26 pp.

NESS 71 An Intercomparison of Meteorological Parameters Derived From Radiosonde and Satellite Vertical Temperature Cross Sections. W. L. Smith and H. M. Woolf, November 1974, 13 pp.